Atmos. Meas. Tech. Discuss., 6, 6645–6684, 2013
www.atmos-meas-tech-discuss.net/6/6645/2013/
doi:10.5194/amtd-6-6645-2013

Atmospheric Measurement Techniques Discussions

Space-based retrieval of NO_2 over biomass burning regions: quantifying and reducing uncertainties

N. Bousserez[1,*]

[1]Dalhousie University, Halifax, N.S., Canada
[*]now at: University of Colorado at Boulder, Boulder, Colorado, USA

Received: 9 June 2013 – Accepted: 10 June 2013 – Published: 22 July 2013

Correspondence to: N. Bousserez (nicolas.bousserez@colorado.edu)

Published by Copernicus Publications on behalf of the European Geosciences Union.

Abstract

The quality of space-based nitrogen dioxide (NO_2) retrievals from solar backscatter depends on a priori knowledge of the vertical profiles of NO_2 and aerosol optical properties. This information is contained in an air mass factor (AMF), which accounts for atmospheric scattering and is used to convert the measured line-of-sight "slant" columns into vertical columns. In this study we investigate the impact of biomass burning emissions on the AMF in order to quantify NO_2 retrieval errors in the Ozone Monitoring Instrument (OMI) products over these sources. Sensitivity analyses are conducted using the Linearized Discrete Ordinate Radiative Transfer (LIDORT) model and the GEOS-Chem chemistry-transport model with an improved daily biomass burning emission inventory. Aircraft in situ data collected during two field campaigns, Arctic Research of the Composition of the Troposphere from Aircraft and Satellites (ARCTAS) and Dust and Biomass-burning Experiment (DABEX), are used to evaluate the modeled aerosol optical properties and NO_2 profiles over Canadian boreal fires and western Africa savanna fires respectively. Biomass burning aerosols increase the AMF by 3 to 15 % over boreal fires, while they decrease the AMF by −10 to −30 % over savanna fires. The presence of an elevated aerosol layer over west Africa due to the Harmattan front explains the negative aerosol effect over this area. The impact of fires on the AMF is driven by the NO_2 shape profile perturbations, which decrease the AMF by −10 to −60 % over both regions. Aerosol and shape factor effects are most sensitive to surface reflectance and clouds. In particular, retrieval errors associated with shape factor uncertainties can increase by a factor of 2 due to the presence of clouds. In contrast with conclusions from previous studies, we demonstrate that in the presence of pre-existing clouds, the effect of aerosols on the AMF cannot be fully accounted for through the modified retrieved cloud parameters. Finally, a new method that uses slant column information to correct for shape factor error in the retrieval is proposed and tested over west African fires.

AMTD

6, 6645–6684, 2013

1 Introduction

Nitrogen oxides ($NO_x = NO_2 + NO$) play a key role in tropospheric chemistry by affecting ozone, atmospheric oxidation, and aerosol formation (Logan, 1983; Finlayson-Pitts and Pitts, 1986). Biomass burning is a significant source of NO_x, but due to the high space and time variability of fire events, this source remains difficult to quantify. Space-based observations of NO_2 offer the possibility to infer global NO_x emissions with a spatial and time coverage that allows to capture such source variability (Leue et al., 2001; Martin et al., 2003). However, top-down estimates of those emissions depend upon the accuracy of the NO_2 observations themselves.

Satellite retrievals of NO_2 columns from solar backscatter are usually based on a two-step process in which slant columns are inferred from spectral fitting and subsequently converted into vertical columns using an air mass factor (AMF) (Richter and Burrows, 2002; Martin et al., 2002). The AMF corrects the measurements for the viewing geometry and the atmospheric scattering effects based on a priori knowledge of the NO_2 profile shapes and atmospheric optical properties. The AMF is the largest source of error in NO_2 retrievals over NO_x sources (Boersma et al., 2004; Martin et al., 2002) and NO_2 profile uncertainty contributes significantly to the AMF error (Russel et al., 2011; Hains et al., 2010). The NO_2 profiles are usually obtained from a chemical transport model (CTM). Because the high spatial and temporal variability of fires is generally not resolved in such models, significant uncertainties in the simulated NO_2 profile are expected. Biomass burning aerosols provide an additional complication to the AMF by altering the scattering properties of the atmosphere (Martin et al., 2003; Leitão et al, 2010). Previous studies have investigated the impact of aerosols on the AMF using modeled profiles of aerosol characteristics (Leitão et al., 2010; Martin et al., 2003). However, it is still unclear how to account for aerosols in the NO_2 retrieval, since cloud products used in AMF calculations are also sensitive to aerosols (Boersma et al., 2011, 2004). In this study, we assess the impact of biomass burning emissions on

AMTD
6, 6645–6684, 2013

the AMF through the modified NO_2 and aerosol profiles and we analyze the interplay between clouds and aerosols in the retrieval algorithm.

The Arctic Research of the Composition of the Troposphere from Aircraft and Satellites (ARCTAS) and The Dust And Biomass EXperiment (DABEX) experiments provide extensive aicraft in situ measurements of NO_2 concentrations and aerosol optical properties over boreal and savanna fires respectively. ARCTAS-B took place in June–July 2008 with a major emphasis on boreal forest fire influences over Canada (Jacob et al., 2009). DABEX, part of the African Monsoon Multidisciplinary Analysis (AMMA) (Redelsperger et al., 2006), took place in January 2006 over West Africa. These two campaigns provide an unprecedented dataset to evaluate modeled aerosol and NO_2 profiles that are used in the AMF calculation. To our knowledge, a comprehensive analysis of NO_2 retrievals over biomass burning supported by detailed aerosol and NO_2 in situ dataset has not been conducted yet.

Section 2 presents the theoretical basis for the AMF algorithm. Section 3 provides a description of the ARCTAS-B and DABEX experiments. Section 4 evaluates the ability of the GEOS-Chem model to reproduce the observed NO_2 profiles and aerosol optical properties. Sections 5 to 8, we analyze the sensitivity of the AMF to biomass burning emissions and investigate the impact of clouds. Finally, in Sect. 9 we present a method to reduce AMF errors associated with NO_2 shape factor uncertainties by applying a correction factor based on slant column information.

2 AMF calculation

The AMF is defined as the ratio of the slant column, which is the total amount of trace gas along an average backscattered path observed by a satellite instrument, to the vertical column of this trace gas. Following Palmer et al. (2001), the AMF can be expressed as

AMTD
6, 6645–6684, 2013

$$\mathrm{AMF} = \mathrm{AMF_G} \int_0^1 \omega(\eta)\, S(\eta)\, d\,\eta \quad (1)$$

where AMF_G is the geometric AMF accounting for the satellite viewing geometry, $S(\eta)$ is the *shape factor*, a dimensionless normalized NO_2 vertical profile, and $\omega(\eta)$ are the scattering weights describing the vertical sensitivity of the radiance observed by the instrument to NO_2.

The AMF formulation we use takes into account cloud-contaminated pixels, as described in Martin et al. (2002). The effective cloud fraction and cloud pressure are retrieved from OMI using the O_2-O_2 algorithm (Acarreta et al., 2004). Surface reflectivity was obtained from a climatology from OMI at 440 nm (Kleipool et al., 2008). Scattering weights are calculated using the Linearized Discrete Ordinate Radiative Transfer (LIDORT) model (Spurr et al., 2001; Spurr, 2002). Shape factors are obtained from a GEOS-Chem simulation described in Appendix A.

3 Observational dataset

3.1 ARCTAS-B campaign

The summer ARCTAS-B campaign took place in late June and early July 2008 (Jacob et al., 2009). The primary goal of this experiment was to better understand the factors driving current changes in Arctic atmospheric composition and climate.

The campaign included the DC-8 research aicraft to measure chemical and radiative properties of the atmosphere. From 26 June to 14 July 2008, the aircraft was based in Cold Lake, Canada (54° N, 110° W), where it sampled many fresh and aged biomass burning plumes (Alvarado et al., 2010). The DC-8 included highly sensitive high-frequency (1–10 s) measurements of key ozone precursors (NO_y, HO_x, PAN,

AMTD
6, 6645–6684, 2013

HCHO) as well as aerosol optical and physical properties. Measurement characteristics for the species considered in this study are summarized Table 1.

Figure 1 shows the DC-8 aircraft flight paths during the ARCTAS-B experiment. Aircraft flights over central Canada mostly targeted biomass burning plumes and sampled a wide range of altitudes, providing valuable information on the influence of fires on tropospheric chemistry. Chemical and optical properties of biomass burning plumes sampled by the DC-8 aircraft during ARCTAS-B were analyzed in detail in Singh et al. (2010) and Alvarado et al. (2010).

3.2 DABEX campaign

The African Monsoon Multidisciplinary Analysis (AMMA) is a major international campaign designed to improve our undestanding of the west African monsoon (Redelsperger et al., 2006). The Dust And Biomass burning EXperiment (DABEX) was part of the Special Observing Period (SOP) dry season (January–February 2006). It was carried out over West Africa by the UK Met Office, which used the FAAM BAe-146 aircraft to perform high-quality in situ measurements of the chemical, optical and physical properties of biomass burning and dust aerosols over western Africa.

Observed optical properties of dust and biomass burning aerosols during DABEX were analyzed in detail in several studies (Johnson et al., 2008a,b; Osborne et al., 2008; Capes et al., 2008). Although valuable information could be obtained from this dataset, characterization of optical properties for fresh biomass burning aerosols were challenging since fresh plumes were usually sampled near the surface where they were also mixed with mineral dust.

Table 2 summarizes the measurement characteristics for the data considered in this study. Figure 2 shows the FAAM BAe-146 flight tracks and altitude during DABEX. The area sampled covered a narrow domain spanning from western Niger, where mineral dust is predominant, to center Benin, where savanna fires occured.

To complete our model evaluation, we also used aerosol optical depth (AOD) and single scattering albedo (SSA) surface in situ data from the Aerosol Robotic Network

AMTD
6, 6645–6684, 2013

(AERONET) network, which consist of sun photometer measurements (Dubovik et al., 2002). Figure 2 shows the location of the stations considered.

4 Model evaluation

The GEOS-Chem model described in Appendix A is a central tool in our analysis of the AMF, since it provides the aerosol and NO_2 profiles used in its calculation. Here we evaluate the simulated aerosol and NO_2 profiles against aircraft in situ measurements from the DABEX and ARCTAS experiments. For this purpose, model outputs were sampled along the flight tracks and filtered to retain only measurements influenced by biomass burning.

For ARCTAS, measurements impacted by biomass burning emissions were identified by enhancements in HCN and CO concentrations greater than 20% of the regional background.

For DABEX, measurements influenced by biomass burning were defined according to Johnson et al. (2008b), who derived the following criteria:

- scattering at 550 nm (green) $> 30.10^{-6}$ m
- Angström exponent > 1

We then performed a sensitivity simulation to ensure that the selected locations were also associated with biomass burning influences in the model. Modeled and observed profiles were subsequently derived by vertically binning the data over the entire ARCTAS (150–80° W; 49–70° N) and DABEX (2° W–8° E; 8–20° N) domains.

Figure 3 shows the shape factor, aerosol extinction and SSA mean profiles during ARCTAS for the DC-8 measurements and the model. There is an overall good agreement between the model and the measurements. The NO_2 shape factor shows a sharp enhancement near the surface due to fire emissions. Model analyses (not shown) suggest that the gradient observed at the top of the troposphere and not seen in the model

AMTD
6, 6645–6684, 2013

is due to an underestimation of lightning NO_x emissions. Aerosol extinction also increases in the boundary layer as a result of biomass burning emissions. The shape and magnitude of the extinction is similar in the model and the measurements. The mean SSA profile is also reasonably well reproduced by the model, with relatively homogeneous values of 0.90–0.95.

Figure 4 shows the profiles of the shape factor, aerosol extinction and aerosol scattering at 450 nm from GEOS-Chem and the DC-8 measurements during DABEX. The modeled and observed shape factors show a significant increase near the surface, similar to the one observed over boreal fires. Aerosol extinction values over savanna fires (~ 0.4–$0.8\,km^{-1}$) are significantly greater than those observed over boreal fires during ARCTAS, which is due to more intense fire emissions over Africa during DABEX. Aerosol extinction and scattering profile shapes are well reproduced by GEOS-Chem. The model underestimation near the surface may be attributed to representativeness errors. Note that infrequent sampling of the boundary layer during DABEX limits confidence in the results near the surface.

Table 3 contains the AOD and SSA columns for GEOS-Chem and the AERONET measurements at several stations in western Africa. The modeled SSA agrees with observations within 0.02 in average, and the modeled AOD within 23 %.

In conclusion, the evaluation of the GEOS-Chem NO_2 profiles and aerosol optical properties over boreal and savanna fires shows that this model can be used to quantify the impact of biomass burning emissions on the AMF.

5 Impact of biomass burning emissions on the AMF

Generally the high spatial and temporal variability of fire emissions is not accurately represented in CTMs. Errors in the simulated aerosol and NO_2 profiles will translate into errors in the AMF estimates. Such errors can be quantified by doing an AMF sensitivity analysis, where aerosols and NO_2 emitted by fires are excluded from the model simulation. Here we define a total biomass burning AMF correction factor (tot_{cor}) as the

AMTD
6, 6645–6684, 2013

product of an aerosol correction due to the effect of biomass burning aerosols ($aero_{cor}$) and a shape factor correction due to the effect of biomass burning NO_x emissions on the NO_2 profile ($shapef_{cor}$):

$$tot_{cor} = aero_{cor}\, shapef_{cor} \quad (2)$$

with:

$$aero_{cor} = \frac{AMF_{bb}^{aero}}{AMF_{bb}^{no\,aero}} \quad \text{and} \quad shapef_{cor} = \frac{AMF_{bb}^{no\,aero}}{AMF_{nobb}^{no\,aero}} \quad (3)$$

where subscripts specify if the shape factors used in the AMF calculation are from a simulation with (bb) or without (nobb) biomass burning emissions, while superscripts specify if the effect of biomass burning aerosols is accounted for (aero) or not (no aero) in the AMF.

Figure 5 shows the mean total biomass burning correction as well as the associated aerosol and shape factor corrections over boreal forest and savanna fires during ARCTAS and DABEX respectively. Only OMI scenes with cloud irradiance fraction $< 5\,\%$ have been retained in order to limit the interference of clouds in the analysis while retaining a statistically significant number of data.

Over boreal fires, the total correction is negative everywhere (-50 to $-10\,\%$) and largely driven by the shape factor correction. Fire emissions reduce the AMF by increasing the NO_2 shape factor near the surface where measurement sensitivity is generally minimum. To the contrary, aerosols increase the AMF due to scattering effects that enhance measurement sensitivity at the surface, but their impact is of smaller amplitude (3–15 %) than the shape factor.

The total correction over savanna fires is similar to the boreal fires case (-60 to $-10\,\%$). While shape factor corrections over boreal and savanna fires are comparable, aerosol corrections over those domains are of opposite sign. Figure 6 shows the mean vertical distribution of aerosol extinctions and NO_2 mixing ratios simulated over boreal

AMTD
6, 6645–6684, 2013

and savanna fires. Over boreal fires, the aerosol and NO_2 layers are co-located and extend from the surface to ~2 km, whereas over savanna fires the top of the aerosol layer reaches ≈4 km altitude, well above the surface NO_2 layer. The simulated vertical extension of the aerosol layer over west Africa is in agreement with the CALIPSO observations for the same period, as shown in Fig. 6. As explained in Haywood et al. (2008), the presence of this elevated aerosol layer is due to the uplift of biomass burning emissions by the Harmattan front. The narrower NO_2 layer stems from the shorter lifetime of NO_x compared to aerosols.

The difference in the relative vertical distribution of aerosols and NO_2 between boreal and savanna fires explains the opposite sign in the aerosol correction. Indeed, surface aerosols mixed with NO_2 tend to increase measurement sensitivity due to light scattering, while aerosols above NO_2 produce a "shielding" effect that decreases measurement sensitivity (Leitão et al., 2010).

In the next two sections we investigate in more detail the sensitivity of the AMF to aerosols and NO_2 shape factor over west African fires.

6 Aerosol correction sensitivity analysis

In this section, we assess the influence of aerosols on the AMF and its dependence to aerosol characteristics (optical properties, profile shape) as well as key retrieval parameters (satellite viewing geometry, surface reflectance, clouds). The reference aerosol and NO_2 profiles for the sensitivity experiment are taken from the GEOS-Chem DABEX simulation over west Africa. Since the model resolution ($2^\circ \times 2.5^\circ$) is much coarser than OMI, and in order to minimize the representativeness error for the NO_2 profiles, we chose model profiles associated with highest fire emissions. Figure 7 shows the simulated NO_2 and aerosol profiles at OMI overpass time (13:30 LT – local time).

The sensitivity of the aerosol correction to aerosol profile shape has been assessed by comparing the correction with and without the elevated aerosol layer, as represented

AMTD
6, 6645–6684, 2013

Fig. 7. As a result of the shielding effect, the aerosol correction decreases from +20 to −30 % in the presence of the elevated aerosol layer.

Figure 8 shows the influence of SSA, solar zenith angle (SZA) and surface reflectance on the aerosol correction for the two types of profile considered. For each of these parameters, the sensitivity of the aerosol correction is similar whether or not the elevated aerosol layer is included. The AMF being a vertical integration of the scattering coefficients weighted by the NO_2 shape factor, its sensitivity is driven by optical properties near the surface where the NO_2 shape factor peaks, which explains the similarities observed.

The aerosol correction is most sensitive to surface reflectance. We observe an exponential decay, which reflects the competing effects of the measurement sensitivity increase due to scattering above the aerosol layer and the shielding effect below it. We see that the relative impact of the shielding effect increases quickly until it reaches an asymptotic limit for surface reflectance > 0.1.

A linear increase of the aerosol correction with SSA is observed, while the viewing geometry (SZA) has negligible impact on the correction, which is consistent with findings by Leitão et al. (2010) over urban areas.

The impact of emissions on the aerosol correction has been assessed by re-scaling the aerosol and NO_2 concentrations within the same surface layer (0–1 km). Figure 8 d) shows that the effect of aerosols on the AMF is almost insensitive to emission intensity. This is due to the AMF increase caused by aerosol scattering effects being counterbalanced by the AMF decrease due to NO_2 shape factor enhancements at the surface. A direct consequence is that the aerosol correction will be only weakly impacted by representativeness errors within one model grid box as long as the aerosol/NO_2 emission factors are homogeneous inside that domain.

Clouds can also indirectly modify the effect of aerosols on the AMF. Figure 9 shows the aerosol correction as a function of cloud irradiance fraction for different AODs, and for the two aerosol profiles considered in Fig. 7. Here the cloud top pressure was set to 460 hPa, which corresponds to the clouds being above the elevated aerosol layer. For

AMTD
6, 6645–6684, 2013

any AOD value, the aerosol correction increases linearly with cloud irradiance fraction, since decreasing the sensitivity below clouds increases the relative impact of aerosols scattering on the AMF. Note that increasing the optical thickness of the elevated aerosol layer does not modify the sensitivity of the aerosol correction to cloud irradiance fraction. This is expected since an elevated aerosol layer will essentially play the same role as an increase in the cloud irradiance fraction in the retrieval. However in the case where NO_2 and aerosols are co-located near the surface, the aerosol correction sensitivity to cloud irradiance fraction increases with AOD. As a result, for AODs > 1, commonly measured over biomass burning events, we see from Fig. 9 that a cloud irradiance fraction of 20 % can lead to an overestimation of a factor 2 in the retrieved NO_2 columns when aerosol effects are not accounted for. It is important to realize that although in our pseudo-experiment the effect of clouds can be separated from the effect of aerosols, in real retrievals they are difficult to disentangle. This important aspect is analyzed in the next section.

7 Do clouds implicitly account for aerosol effects?

Aerosols may impact the retrieval of cloud parameters. Boersma et al. (2011, 2004) suggested that the effect of aerosols on the AMF was implicitly accounted for through the modified cloud parameters. They recommended to not use an explicit aerosol correction in the AMF, since it could potentially be detrimental to the quality of the NO_2 retrievals. However the results presented in their studies were derived using specific assumptions on the retrieved scene (clear sky, exponentially decreasing shape profiles for aerosols and NO_2), and this conclusion may not be valid in all cases. A particular case is the presence of pre-existing clouds in the scene, which as we showed in Sect. 6 modifies the effect of aerosols on the AMF.

Let us assume as Boersma et al. (2004) that under clear-sky conditions the aerosol-induced perturbation of the cloud parameters produces a similar effect on the AMF than an explicit aerosol correction. From our previous results, if true clouds are added

AMTD
6, 6645–6684, 2013

to the scene, the aerosol correction will increase. Since this aerosol correction perturbation is not associated with any perturbation of the retrieved cloud parameters (it is an artifact of clouds), we see that in the presence of true clouds the implicit aerosol correction cannot fully account for the explicit aerosol effects. This result suggests that the impact of aerosols should be explicitly accounted for in the AMF calculation. In practice though, this would require both a good knowledge of the aerosol vertical distribution and accurately quantifying its impact on the OMI cloud retrieval.

8 Shape factor correction sensitivity analysis

The impact of biomass burning emissions on the AMF through the modified NO_2 shape factor is also altered by changes in other retrieval parameters. Figure 10 shows the sensitivity of the shape factor correction to cloud irradiance fraction and surface reflectance. The shape factor correction decreases almost linearly with cloud fraction. For a cloud fraction of 30 %, which is the threshold currently used in operational OMI NO_2 retrievals, AMF shape factor errors can be amplified by a factor 2. Therefore, using a lower threshold for the cloud screening over regions with uncertain NO_x emissions (like biomass burning areas) might be critical in order to reduce retrieval errors.

Similarly to the aerosol correction, the shape factor correction is highly sensitivite to surface reflectance at low values. For surface reflectances typically found over savanna or boreal forest areas (0.03–0.05), our results show that retrieval errors associated with shape factor uncertainties can be as high as 60 %. This highlights the need for using high spatial resolution surface albedo climatology in the AMF calculation, as recently included in an improved OMI NO_2 product by Boersma et al. (2011).

AMTD
6, 6645–6684, 2013

9 Measurement-based shape factor correction

9.1 Methodology

In the previous section we showed that errors in the simulated NO_2 shape factor are the dominant source of error in the AMF over biomass burning regions. Of concern is that current operational OMI NO_2 retrievals use climatological NO_2 profiles that cannot represent the true spatial and temporal variation needed for accurate retrievals. Here we investigate a method to infer shape factor corrections using measurement information. As explained in Sect. 2, measurement information is contained in the slant columns, whereas AMFs are calculated using a priori information, usually from a CTM. Over high NO_x sources like fires, most of the NO_2 column will be concentrated in the boundary layer. Local variability of the slant columns will therefore be primarily affected by variability of the lower part of the NO_2 profile.

Here we use this property to establish a relationship between the shape factor correction and a slant column perturbation, defined as the relative increase of the slant column with respect to a case without biomass burning emissions. Slant columns and shape factor corrections are computed using a pseudo-retrieval experiment, in which OMI NO_2 averaging kernels are applied to the GEOS-Chem NO_2 profiles (Eskes et al., 2003). Two GEOS-Chem simulations, one using daily biomass burning emissions (BB_{sim}), and one with biomass burning emissions turned off ($NOBB_{sim}$) are used to generate three types of pseudo NO_2 retrievals:

- *A*, of BB_{sim} using NO_2 shape factors from $NOBB_{sim}$;
- *B*, of $NOBB_{sim}$ using NO_2 shape factors from $NOBB_{sim}$;
- *C*, of BB_{sim} using NO_2 shape factors from BB_{sim}.

Note that using a perfect shape factor in *B* and *C* (the one corresponding to the column retrieved) results in *B* and *C* being the actual GEOS-Chem columns.

We further define:

AMTD
6, 6645–6684, 2013

– $\Delta NO_2 = \frac{A-B}{B}$, the relative NO_2 column increase compared to the case without biomass burning;

– NO_2 correction factor $= \frac{C}{A}$.

The dependence of ΔNO_2 to measurement information can be make explicit by rewriting: $\Delta NO_2 = \frac{Slt_A - Slt_B}{Slt_B}$.

Figure 11 shows the relationship between ΔNO_2 and the NO_2 correction factor over western Africa fires during DABEX. The correction factor increases with ΔNO_2 with a "saturation effect" for $\Delta NO_2 > 4$, where the NO_2 correction is almost constant ($= 3$). Further increasing NO_x emissions above this threshold does not change the shape factor since almost the totality of the NO_2 column is already concentrated in the mixed layer. The relationship between the NO_2 correction factor and ΔNO_2 can be well approximated by the following logarithmic fit:

$$NO_2 \text{ correction factor} = \log\left(3.4\,\Delta NO_2 + 2.2\right). \quad (4)$$

The above formula can be applied to real retrievals by replacing the pseudo NO_2 slant columns in A by the measured NO_2 slant columns and assuming the reference column in B is a good approximation of what would be the measured slant column without the fire source. Such measurement-based shape factor correction is intended to reduce uncertainties related to both representativeness errors and misrepresentation of the location and time of fires in the model simulation.

9.2 Results

Figure 12 shows the average NO_2 tropospheric column distribution over west Africa during DABEX from the OMI DP GC product (Lamsal et al., 2010), which consists in replacing the TM4 NO_2 shape profile by the GEOS-Chem NO_2 shape profile in the DOMINO product (Boersma et al., 2007). Here NO_2 profiles are obtained from

AMTD
6, 6645–6684, 2013

the DABEX simulation, using the FLAMBE daily biomass burning emissions inventory. MODIS AOD over potential biomass burning NO_x sources (OMI DP GC NO_2 columns $> 10^{15}$ molec cm^{-2}) as well as the percentage change in the OMI DP GC NO_2 columns associated with the measurement-based correction are also shown. Corrections to the original OMI NO_2 retrieval can reach more than 40 % over fires, where MODIS AODs are maximum. The fact that only positive correction are observed reflects a low bias in the modeled shape factor at the surface, which is likely related to an overall underestimation of biomass burning emissions over west Africa.

The standard deviation of the NO_2 correction in figure (Fig. 12) can be interpreted as the error associated with the logarithmic fit approximation (Eq. 4). Although large uncertainties can be observed, one sees that they are all significantly smaller than the retrieval error associated with missing biomass burning sources. We therefore recommend using the proposed correction for NO_2 retrievals over biomass burning regions. Note that generalization of this formula to retrievals over other areas (e.g. urban) would require more investigation, since it is possible that very different characteristics in parameters such as surface reflectance could result in a different relationship. Also, due to the lack of aircraft measurements in the boundary layer during DABEX, our approach cannot be rigorously evaluated using in situ-derived NO_2 columns. A study using in situ data from other aircraft campaigns (e.g. INTEX-A, INTEX-B and PAVE) would allow to properly evaluate the robustness of the above formula as well as to better characterize the errors.

10 Conclusions

In this work, we analyze the sensitivity of the air mass factor (AMF) to biomass burning emissions in order to better characterize and understand NO_2 retrieval uncertainties over fire areas. The dependence of the AMF to aerosols and NO_2 shape profiles is investigated in details using outputs from the GEOS-Chem model with daily-resolved fire emissions (FLAMBE) over boreal and savanna fires. Simulated aerosol optical prop-

AMTD
6, 6645–6684, 2013

erties and NO_2 profiles were validated against aircraft in situ measurements from the ARCTAS-B (Canadian fires, summer 2008) and DABEX (western Africa fires, winter 2006) campaigns.

Biomass burning aerosols increase the AMF by 3 to 15 % over Canadian boreal fires, and decrease it by −10 to −35 % over western Africa savanna fires. Co-localized aerosol and NO_2 layers at the surface over boreal fires explains the increase in measurement sensitivity due to aerosol scattering. Over west Africa, uplift of biomass burning emissions by the Harmattan front generates an elevated aerosol layer that decreases measurement sensitivity by shielding effect. Over both regions, the impact of fire-induced shape factor perturbations on the AMF range from −10 to −60 %.

We further analyzed the influence of several retrieval parameters (surface reflectance, clouds, viewing geometry) on the AMF sensitivity to aerosols and shape factors. Both aerosol and shape factor effects are most sensitive to surface reflectance. Our results show that using accurate surface reflectances is critical to reduce retrieval errors over biomass burning areas. Our sensitivity study also shows that for a given NO_2/aerosols emission ratio the effect of aerosols on the AMF is not sensitive to the intensity of emissions, which suggests that representativeness errors are not significant in this case.

We found that the impact of biomass burning emissions on the AMF is very sensitive to clouds. In particular, shape factor-related AMF errors can increase by a factor of 2 due to the presence of clouds in the retrieval. On the other hand, the OMI cloud retrieval is sensitive to aerosols, and previous studies suggested that the aerosol effect on the AMF was implicitly accounted for through the modified cloud parameters in the NO_2 retrieval. Here we demonstrate that in the case of pre-existing clouds, this implicit cloud correction cannot fully account for an explicit aerosol correction. Therefore, more investigations are needed in order to better understand in what cases including an explicit aerosol correction reduces retrieval errors compared to a retrieval that does not account for aerosol effects.

AMTD
6, 6645–6684, 2013

Finally, we developed a new method to reduce NO_2 retrieval errors associated with misrepresentations of the NO_2 shape factors. A measurement-based shape factor correction, based on the local sensitivity of the NO_2 slant column to NO_2 sources, has been proposed and applied to real OMI NO_2 measurements over west Africa. The results show an increase of up to 40 % compared to the original tropospheric NO_2 column retrievals over highest fire emissions. In practice, this methodology could be extended to any type of NO_x source, with possible adaptations of the formula over areas with very different retrieval characteristics (e.g. surface reflectance). Future studies using in situ-derived NO_2 columns over urban and biomass burning regions would allow a proper evaluation of this method and to assess its relevance for existing operational OMI NO_2 retrievals.

Appendix A

GEOS-Chem simulations

GEOS-Chem is a global 3-D chemical transport model driven by assimilated meteorological observations from the Goddard Earth Observing System (GEOS) of the NASA Global Modeling and Assimilation Office (GMAO) (www.geos-chem.org; Bey et al., 2001). We use the GEOS-5 meteorological data regrided to 2°, latitude × 2.5°, longitude, with 47 vertical layers. For both the DABEX and ARCTAS-B period we use the NRT-ARCTAS GEOS-Chem simulation, which was originally developed in support of the ARCTAS mission and is based on GEOS-Chem v8-01-01 with minor modifications (Mao et al., 2010). The simulation includes ozone-NOx-HOx-VOC-aerosol chemistry as described in Park et al. (2005).

A daily biomass burning emission inventory with 1° × 1° resolution obtained from Fire Locating and Monitoring of Burning Emissions (FLAMBE) (Reid et al., 2009) is used to capture the high spatial and temporal variability of the fire emissions. The FLAMBE product is constrained by GOES and MODIS fires count data and provides daily global

AMTD
6, 6645–6684, 2013

smoke and carbon emissions. Emissions for black carbon and organic carbon species in GEOS-Chem are obtained by applying emission factors to the FLAMBE smoke emissions, while emissions for other species, including NO_x, are derived by applying emission factors to the carbon emissions. Emission factors are those proposed by Andreae and Merlet (2001). Further information about the biomass burning emissions in the model can be found in Fisher et al. (2010).

Dust aerosol concentrations can be significant over west Africa due to transport from the Sahara desert. The mineral dust module in GEOS-Chem simulates the mobilization of dust from the Earth's surface, gravitational settling, and wet and dry deposition as described in Fairlie et al. (2007).

For our ARCTAS simulation, a 70 % decrease of carbon emissions and a 60 % decrease of smoke emissions in the FLAMBE inventory, as well as the use of an extra-tropical forest fires NO_x emission factor of 0.42 g NO/kg DM (Alvarado et al., 2010) were required in order to match the aircraft in situ observations.

Acknowledgements. This work was supported by the Canadian Foundation for Climate and Atmospheric Sciences.

References

Acarreta, J., De Haan, J., and Stammes, P.: Cloud pressure retrieval using the O_2-O_2 absorption band at 477 nm, J. Geophys. Res.-Atmos., 109, D05204, doi:10.1029/2003JD003915, 2004.

Alvarado, M. J., Logan, J. A., Mao, J., Apel, E., Riemer, D., Blake, D., Cohen, R. C., Min, K.-E., Perring, A. E., Browne, E. C., Wooldridge, P. J., Diskin, G. S., Sachse, G. W., Fuelberg, H., Sessions, W. R., Harrigan, D. L., Huey, G., Liao, J., Case-Hanks, A., Jimenez, J. L., Cubison, M. J., Vay, S. A., Weinheimer, A. J., Knapp, D. J., Montzka, D. D., Flocke, F. M., Pollack, I. B., Wennberg, P. O., Kurten, A., Crounse, J., St. Clair, J. M., Wisthaler, A., Mikoviny, T., Yantosca, R. M., Carouge, C. C., and Le Sager, P.: Nitrogen oxides and PAN in plumes from boreal fires during ARCTAS-B and their impact on ozone: an integrated analysis of aircraft and satellite observations, Atmos. Chem. Phys., 10, 9739–9760, doi:10.5194/acp-10-9739-2010, 2010.

AMTD
6, 6645–6684, 2013

Bey, I., Jacob, D., Yantosca, R., Logan, J., Field, B., Fiore, A., Li, Q., Liu, H., Mickley, L., and Schultz, M.: Global modeling of tropospheric chemistry with assimilated meteorology: Model description and evaluation, J. Geophys. Res.-Atmos., 106, 23073–23095, doi:10.1029/2001JD000807, 2001.

Boersma, K. F., Eskes, H., and Brinksma, E.: Error analysis for tropospheric NO_2 retrieval from space, J. Geophys. Res.-Atmos., 109, D04311, doi:10.1029/2003JD003962, 2004.

Boersma, K. F., Eskes, H. J., Veefkind, J. P., Brinksma, E. J., van der A, R. J., Sneep, M., van den Oord, G. H. J., Levelt, P. F., Stammes, P., Gleason, J. F., and Bucsela, E. J.: Near-real time retrieval of tropospheric NO_2 from OMI, Atmos. Chem. Phys., 7, 2103–2118, doi:10.5194/acp-7-2103-2007, 2007.

Boersma, K. F., Eskes, H. J., Dirksen, R. J., van der A, R. J., Veefkind, J. P., Stammes, P., Huijnen, V., Kleipool, Q. L., Sneep, M., Claas, J., Leitão, J., Richter, A., Zhou, Y., and Brunner, D.: An improved tropospheric NO_2 column retrieval algorithm for the Ozone Monitoring Instrument, Atmos. Meas. Tech., 4, 1905–1928, doi:10.5194/amt-4-1905-2011, 2011.

Capes, G., Johnson, B., McFiggans, G., Williams, P. I., Haywood, J., and Coe, H.: Aging of biomass burning aerosols over West Africa: Aircraft measurements of chemical composition, microphysical properties, and emission ratios, J. Geophys. Res.-Atmos., 113, D00C15, doi:10.1029/2008JD009845, 2008.

Dubovik, O., Holben, B., Eck, T., Smirnov, A., Kaufman, Y., King, M., Tanre, D., and Slutsker, I.: Variability of absorption and optical properties of key aerosol types observed in worldwide locations, J. Atmos. Sci., 59, 590–608, doi:10.1175/1520-0469(2002)059, 2002.

Fairlie, T. D., Jacob, D. J., and Park, R. J.: The impact of transpacific transport of mineral dust in the United States, Atmos. Environ., 41, 1251–1266, doi:10.1016/j.atmosenv.2006.09.048, 2007.

Fisher, J. A., Jacob, D. J., Purdy, M. T., Kopacz, M., Le Sager, P., Carouge, C., Holmes, C. D., Yantosca, R. M., Batchelor, R. L., Strong, K., Diskin, G. S., Fuelberg, H. E., Holloway, J. S., Hyer, E. J., McMillan, W. W., Warner, J., Streets, D. G., Zhang, Q., Wang, Y., and Wu, S.: Source attribution and interannual variability of Arctic pollution in spring constrained by aircraft (ARCTAS, ARCPAC) and satellite (AIRS) observations of carbon monoxide, Atmos. Chem. Phys., 10, 977–996, doi:10.5194/acp-10-977-2010, 2010.

Hains, J. C., Boersma, K. F., Kroon, M., Dirksen, R. J., Cohen, R. C., Perring, A. E., Bucsela, E., Volten, H., Swart, D. P. J., Richter, A., Wittrock, F., Schoenhardt, A., Wagner, T., Ibrahim, O. W., van Roozendael, M., Pinardi, G., Gleason, J. F., Veefkind, J. P., and Lev-

AMTD
6, 6645–6684, 2013

elt, P.: Testing and improving OMI DOMINO tropospheric NO_2 using observations from the DANDELIONS and INTEX-B validation campaigns, J. Geophys. Res.-Atmos., 115, D05301, doi:10.1029/2009JD012399, 2010.

Haywood, J. M., Pelon, J., Formenti, P., Bharmal, N., Brooks, M., Capes, G., Chazette, P., Chou, C., Christopher, S., Coe, H., Cuesta, J., Derimian, Y., Desboeufs, K., Greed, G., Harrison, M., Heese, B., Highwood, E. J., Johnson, B., Mallet, M., Marticorena, B., Marsham, J., Milton, S., Myhre, G., Osborne, S. R., Parker, D. J., Rajot, J., Schulz, M., Slingo, A., Tanre, D., and Tulet, P.: Overview of the Dust and Biomass-burning Experiment and African Monsoon Multidisciplinary Analysis Special Observing Period-0, J. Geophys. Res.-Atmos., 113, D00C17, doi:10.1029/2008JD010077, 2008.

Jacob, D. J., Crawford, J. H., Maring, H., Clarke, A. D., Dibb, J. E., Emmons, L. K., Ferrare, R. A., Hostetler, C. A., Russell, P. B., Singh, H. B., Thompson, A. M., Shaw, G. E., McCauley, E., Pederson, J. R., and Fisher, J. A.: The Arctic Research of the Composition of the Troposphere from Aircraft and Satellites (ARCTAS) mission: design, execution, and first results, Atmos. Chem. Phys., 10, 5191–5212, doi:10.5194/acp-10-5191-2010, 2010.

Johnson, B. T., Heese, B., McFarlane, S. A., Chazette, P., Jones, A., and Bellouin, N.: Vertical distribution and radiative effects of mineral dust and biomass burning aerosol over West Africa during DABEX, J. Geophys. Res.-Atmos., 113, D00C12, doi:10.1029/2008JD009848, 2008a.

Johnson, B. T., Osborne, S. R., Haywood, J. M., and Harrison, M. A. J.: Aircraft measurements of biomass burning aerosol over West Africa during DABEX, J. Geophys. Res.-Atmos., 113, D00C06, doi:10.1029/2007JD009451, 2008b.

Kleipool, Q. L., Dobber, M. R., de Haan, J. F., and Levelt, P. F.: Earth surface reflectance climatology from 3 years of OMI data, J. Geophys. Res.-Atmos., 113, D18308, doi:10.1029/2008JD010290, 2008.

Lamsal, L. N., Martin, R. V., van Donkelaar, A., Celarier, E. A., Bucsela, E. J., Boersma, K. F., Dirksen, R., Luo, C., and Wang, Y.: Indirect validation of tropospheric nitrogen dioxide retrieved from the OMI satellite instrument: Insight into the seasonal variation of nitrogen oxides at northern midlatitudes, J. Geophys. Res.-Atmos., 115, D05302, doi:10.1029/2009JD013351, 2010.

Leitão, J., Richter, A., Vrekoussis, M., Kokhanovsky, A., Zhang, Q. J., Beekmann, M., and Burrows, J. P.: On the improvement of NO_2 satellite retrievals – aerosol impact on the airmass factors, Atmos. Meas. Tech., 3, 475–493, doi:10.5194/amt-3-475-2010, 2010.

AMTD
6, 6645–6684, 2013

Mao, J., Jacob, D. J., Evans, M. J., Olson, J. R., Ren, X., Brune, W. H., St. Clair, J. M., Crounse, J. D., Spencer, K. M., Beaver, M. R., Wennberg, P. O., Cubison, M. J., Jimenez, J. L., Fried, A., Weibring, P., Walega, J. G., Hall, S. R., Weinheimer, A. J., Cohen, R. C., Chen, G., Crawford, J. H., McNaughton, C., Clarke, A. D., Jaeglé, L., Fisher, J. A., Yantosca, R. M., Le Sager, P., and Carouge, C.: Chemistry of hydrogen oxide radicals (HO_x) in the Arctic troposphere in spring, Atmos. Chem. Phys., 10, 5823–5838, doi:10.5194/acp-10-5823-2010, 2010.

Martin, R., Chance, K., Jacob, D., Kurosu, T., Spurr, R., Bucsela, E., Gleason, J., Palmer, P., Bey, I., Fiore, A., Li, Q., Yantosca, R., and Koelemeijer, R.: An improved retrieval of tropospheric nitrogen dioxide from GOME, J. Geophys. Res.-Atmos., 107, 4437, doi:10.1029/2001JD001027, 2002.

Martin, R., Jacob, D., Chance, K., Kurosu, T., Palmer, P., and Evans, M.: Global inventory of nitrogen oxide emissions constrained by space-based observations of NO_2 columns, J. Geophys. Res.-Atmos., 108(D17), 4537, doi:10.1029/2003JD003453, 2003.

Osborne, S. R., Johnson, B. T., Haywood, J. M., Baran, A. J., Harrison, M. A. J., and McConnell, C. L.: Physical and optical properties of mineral dust aerosol during the Dust and Biomass-burning Experiment, J. Geophys. Res.-Atmos., 113, D00C03, doi:10.1029/2007JD009551, 2008.

Palmer, P., Jacob, D., Chance, K., Martin, R., Spurr, R., Kurosu, T., Bey, I., Yantosca, R., Fiore, A., and Li, Q.: Air mass factor formulation for spectroscopic measurements from satellites: Application to formaldehyde retrievals from the Global Ozone Monitoring Experiment, J. Geophys. Res.-Atmos., 106, 14539–14550, doi:10.1029/2000JD900772, 2001.

Park, R., Jacob, D., Palmer, P., Clarke, A., Weber, R., Zondlo, M., Eisele, F., Bandy, A., Thornton, D., Sachse, G., and Bond, T.: Export efficiency of black carbon aerosol in continental outflow: Global implications, J. Geophys. Res.-Atmos., 110, D11205, doi:10.1029/2004JD005432, 2005.

Redelsperger, J., Thorncroft, C. D., Diedhiou, A., Lebel, T., Parker, D. J., and Polcher, J.: African monsoon multidisciplinary analysis – An international research project and field campaign, B. Am. Meteorol. Soc., 87, 1739–1746, doi:10.1175/BAMS-87-12-1739, 2006.

Reid, J. S., Hyer, E. J., Prins, E. M., Westphal, D. L., Zhang, J., Wang, J., Christopher, S. A., Curtis, C. A., Schmidt, C. C., Eleuterio, D. P., Richardson, K. A., and Hoffman, J. P.: Global Monitoring and Forecasting of Biomass-Burning Smoke: Description of and Lessons From the Fire Locating and Modeling of Burning Emissions (FLAMBE) Program, IEEE J. Sel. Top. Appl. Earth Observ. Remote Sens., 2, 144–162, doi:10.1109/JSTARS.2009.2027443, 2009.

AMTD
6, 6645–6684, 2013

Richter, A. and Burrows, J.: Tropospheric NO_2 from GOME measurements, Remote Sensing of Trace Constituents in the Lower Stratosphere, Troposphere and the Earth's Surface: Global Observations, Air Poll. Atmos. Correct., 29, 1673–1683, doi:10.1016/S0273-1177(02)00100-X, 2002.

Russell, A. R., Perring, A. E., Valin, L. C., Bucsela, E. J., Browne, E. C., Wooldridge, P. J., and Cohen, R. C.: A high spatial resolution retrieval of NO_2 column densities from OMI: method and evaluation, Atmos. Chem. Phys., 11, 8543–8554, doi:10.5194/acp-11-8543-2011, 2011.

Singh, H. B., Anderson, B. E., Brune, W. H., Cai, C., Cohen, R. C., Crawford, J. H., Cubison, M. J., Czech, E. P., Emmons, L., Fuelberg, H. E., Huey, G., Jacob, D. J., Jimenez, J. L., Kaduwela, A., Kondo, Y., Mao, J., Olson, J. R., Sachse, G. W., Vay, S. A., Weinheimer, A., Wennberg, P. O., Wisthaler, A., and ARCTAS Sci Team: Pollution influences on atmospheric composition and chemistry at high northern latitudes: Boreal and California forest fire emissions, Atmos. Environ., 44, 4553-4564, doi:10.1016/j.atmosenv.2010.08.026, 2010.

Spurr, R.: Simultaneous derivation of intensities and weighting functions in a general pseudo-spherical discrete ordinate radiative transfer treatment, J. Quant. Spectrosc. Ra., 75, 129–175, doi:10.1016/S0022-4073(01)00245-X, 2002.

Spurr, R., Kurosu, T., and Chance, K.: A linearized discrete ordinate radiative transfer model for atmospheric remote-sensing retrieval, J. Quant. Spectrosc. Ra., 68, 689–735, doi:10.1016/S0022-4073(00)00055-8, 2001.

AMTD
6, 6645–6684, 2013

Table 1. DC-8 research payload during ARCTAS-B for the species considered in this study.

Species, parameters	Method	Investigator	Reference
NO_2	TD-LIF*	R. Cohen, UC Berkeley	Cleary et al. (2002)
Aerosol optical properties	Nephelometer, PSPAP	B. Anderson, NASA LaRC	Anderson et al. (1998)
Black carbon aerosol	SP2**	Y. Kondo, U. Tokyo	Moteki and Kondo (2007, 2008)

* TD-LIF = Thermal-Dissociation Laser Induced Fluorescence, ** SP2 = Single Particle Soot Photometer.

AMTD
6, 6645–6684, 2013

Table 2. FAAM BAe-146 research payload during DABEX for the species considered in this study.

Species, parameters	Instrument	Comment
NO_2	TECO 42	detection limit < 2 ppbv
Aerosol absorption	Radiance Research PSAP	wavelength, $\lambda = 0.568$ mum
Dry aerosol scattering	TSI 3563 Nephelometer	$\lambda = 0.45, 0.55, 0.70$ µm

AMTD
6, 6645–6684, 2013

Table 3. Simulated and observed mean SSA and AOD columns at several AERONET sites during DABEX.

	SSA	AOD
Banizoumbou (13° N, 2° E)		
AERONET	0.84	0.75
GC	0.84	0.63
Djougou (9° N, 1° E)		
AERONET	0.82	1.05
GC	0.84	1.19
IER-Cinzana (13° N, 5° W)		
AERONET	0.83	0.65
GC	0.85	0.61
Ilorin (8° N, 4° E)		
AERONET	0.86	1.37
GC	0.89	0.80
DMN-Maine Soroa (13° N, 12° E)		
AERONET	0.88	0.80
GC	0.82	1.23
Dakar (14° N, 16° W)		
AERONET	0.83	0.84
GC	0.85	0.95

AMTD
6, 6645–6684, 2013

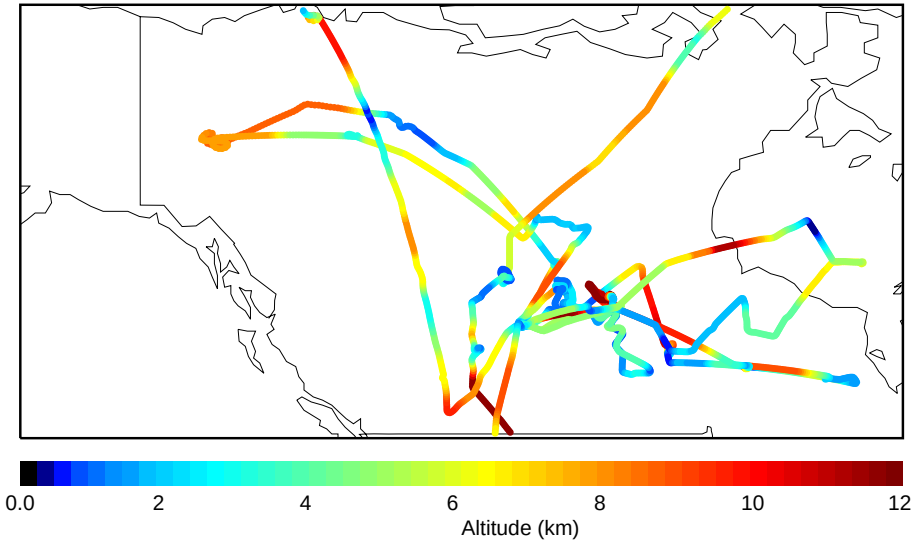

Fig. 1. NASA DC-8 flight tracks during ARCTAS-B over Canada. The color indicates the altitude of the aircraft.

AMTD
6, 6645–6684, 2013

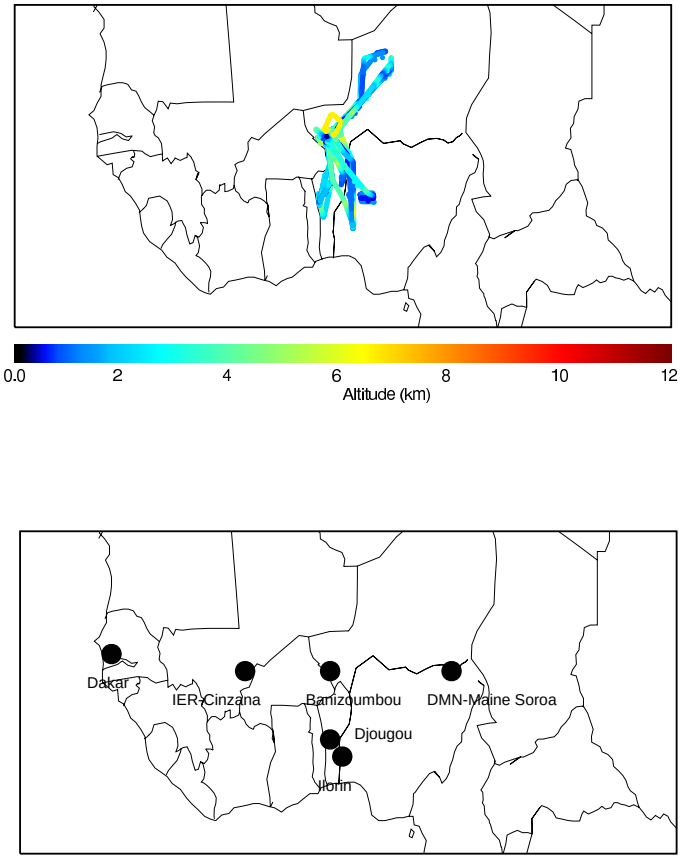

Fig. 2. Top panel: FAAM BAe-146 flight tracks during DABEX. The color indicates the altitude of the aircraft. Bottom panel: locations and names of the AERONET stations considered in this study.

AMTD
6, 6645–6684, 2013

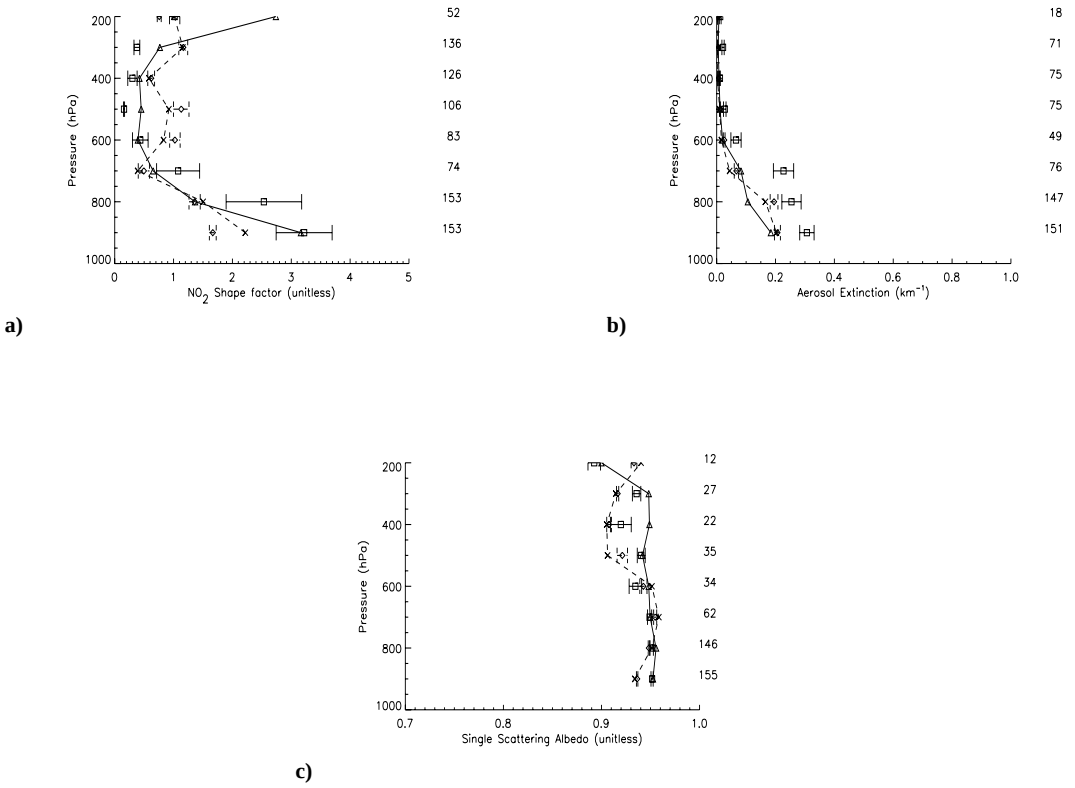

Fig. 3. Simulated and observed vertical profiles of NO_2 shape factors **(a)**, aerosol extinction **(b)**, and single scattering albedo **(c)** during ARCTAS. Model median values (dashed line) are represented by crosses and measurements median values (solid line) by triangles. Model mean values are represented by diamonds and measurements mean values by square. Bars indicate the standard error of the mean at each altitude level.

AMTD
6, 6645–6684, 2013

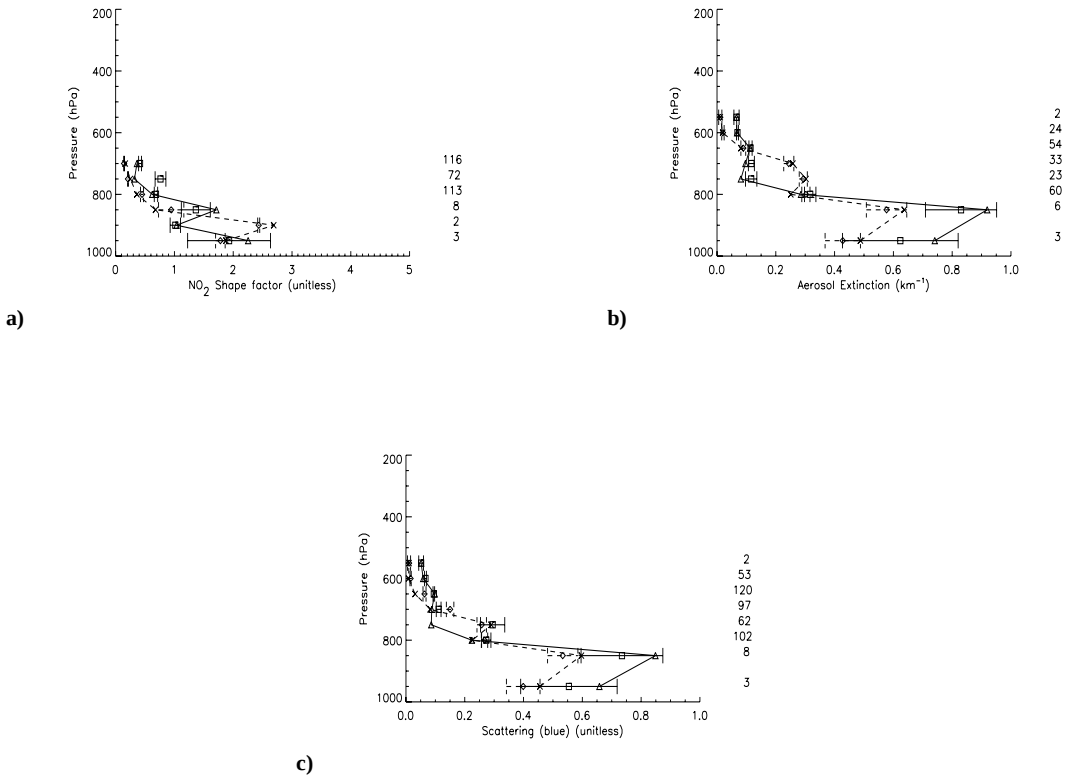

Fig. 4. Simulated and observed vertical profiles of NO_2 shape factors **(a)**, aerosol extinction **(b)**, and aerosol scattering at 450 nm (blue) **(c)** during DABEX. Model median values (dashed line) are represented by crosses and measurements median values (solid line) by triangles. Model mean values are represented by diamonds and measurements mean values by square. Bars indicate the standard error of the mean at each altitude level.

AMTD
6, 6645–6684, 2013

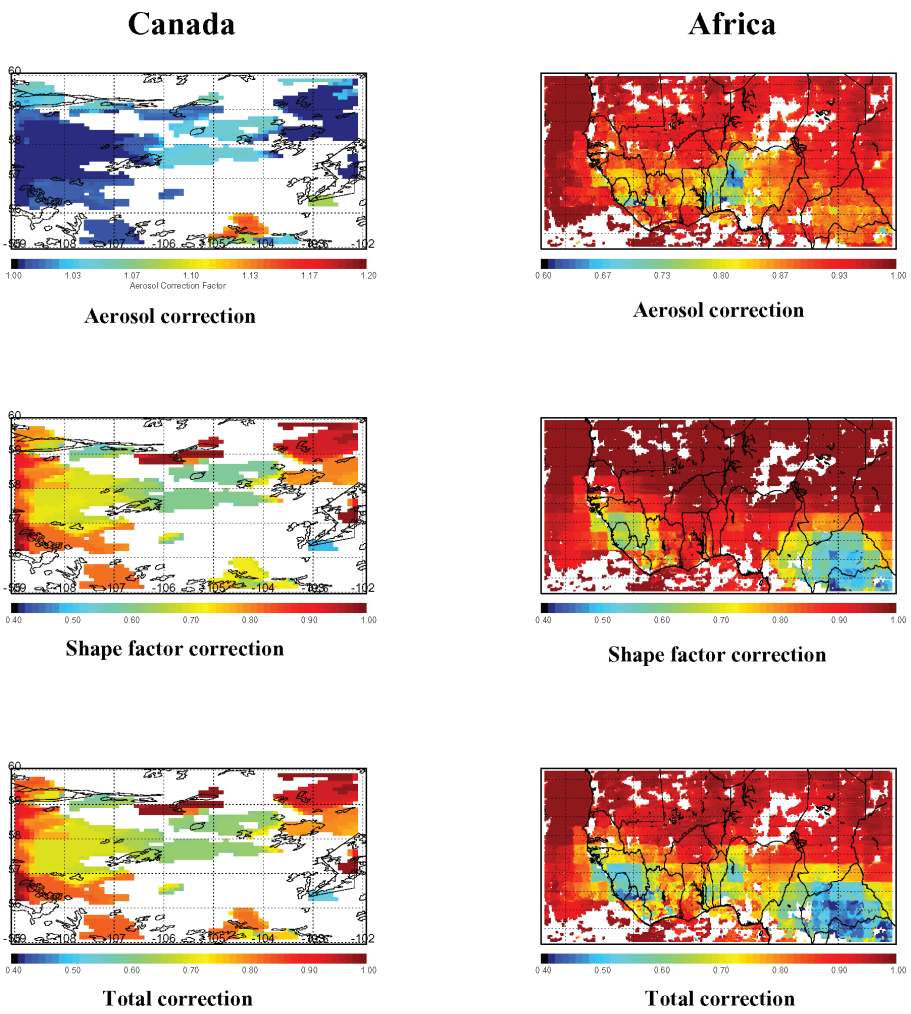

AMTD
6, 6645–6684, 2013

Retrieval of NO_2 over biomass burning regions

N. Bousserez

Fig. 5. Mean AMF aerosol correction, shape factor correction and total correction over Canadian fires during ARCTAS (30 June–10 July 2008) (left column) and western Africa fires during DABEX (13 January–2 February 2006) (right column). Retrievals with a cloud irradiance fraction > 5 % have been excluded.

AMTD
6, 6645–6684, 2013

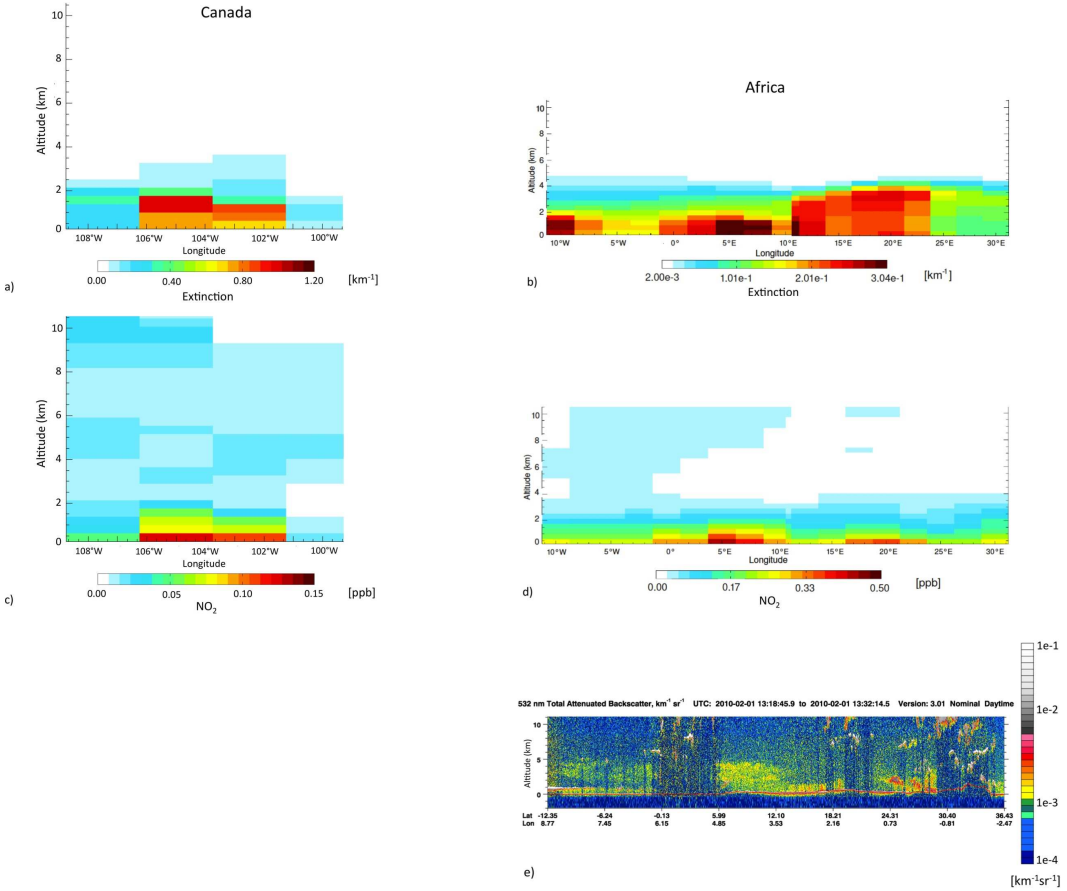

AMTD
6, 6645–6684, 2013

Retrieval of NO_2 over biomass burning regions

N. Bousserez

Fig. 6. Mean vertical distribution of the simulated aerosol extinction and NO_2 mixing ratio over Canada (109° W–99° W, 56° N) during ARCTAS (left column) and west Africa (10° W–30° E, 6° N–12° N) during DABEX (right column). Model outputs have been sampled at OMI overpass time (01:30 LT – local time) and averaged over land only. Bottom panel: a transect of the CALIPSO total attenuated backscatter (532 nm) on 1 February 2010 showing the vertical extension of the aerosol layer over west African fires.

AMTD
6, 6645–6684, 2013

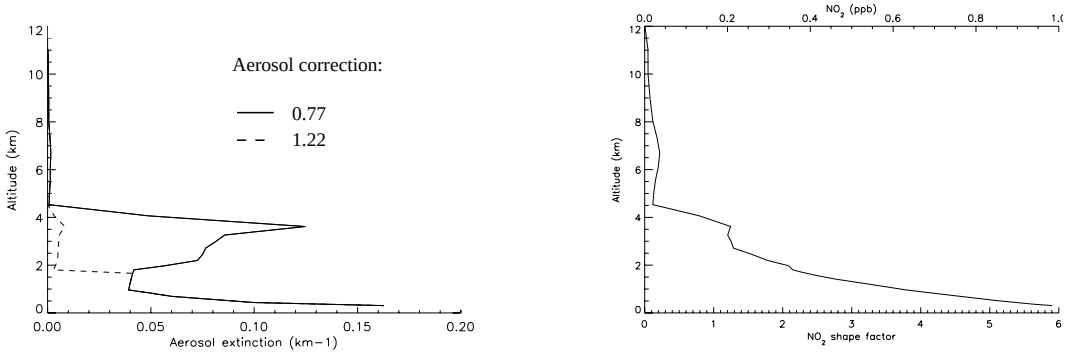

Fig. 7. Left panel: GEOS-Chem aerosol extinction profile with (solid) and without (dashed) the elevated aerosol layer for a single grid cell over west Africa fires at OMI overpass time (01:30 LT). The aerosol correction values corresponding to each type of aerosol profile are reported on the figure. Right panel: GEOS-Chem NO_2 profile shape for the same grid cell.

AMTD
6, 6645–6684, 2013

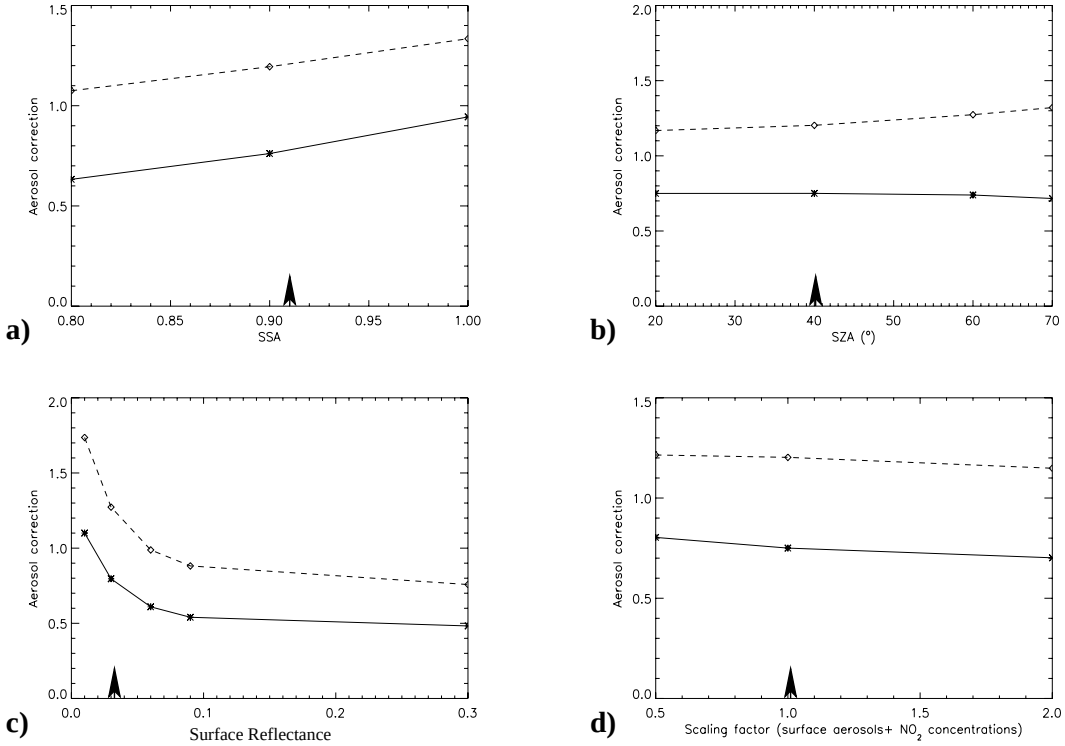

Fig. 8. Aerosol correction sensitivity to: **(a)** single scattering albedo, **(b)** solar zenital angle, **(c)** surface reflectance, and **(d)** emissions (aerosol and NO_2 surface concentration rescaling). Solid and dashed lines correspond respectively to the case with and without the elevated aerosol layer. For each parameter, the arrow indicates the value corresponding to the reference case from the DABEX simulation.

AMTD
6, 6645–6684, 2013

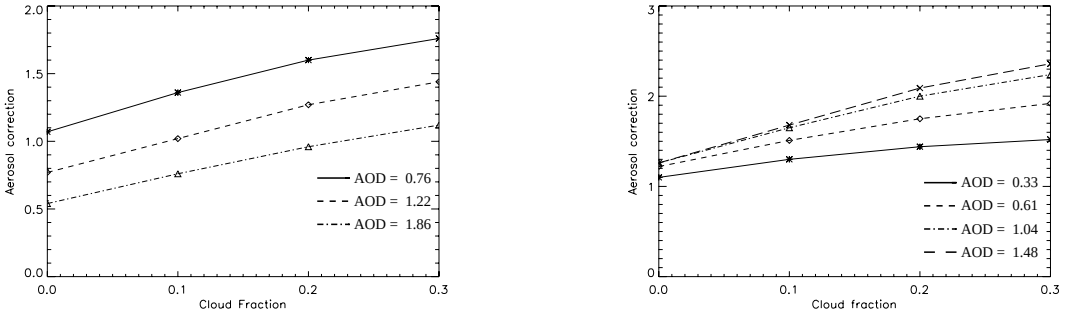

Fig. 9. Aerosol correction sensitivity to cloud irradiance fraction for different AODs. The left panel corresponds to the case with an elevated aerosol layer, while the right panel corresponds to a surface-only aerosol layer. Different AODs were obtained by rescaling either the elevated aerosol layer (left panel) or the surface aerosol layer (right panel).

AMTD
6, 6645–6684, 2013

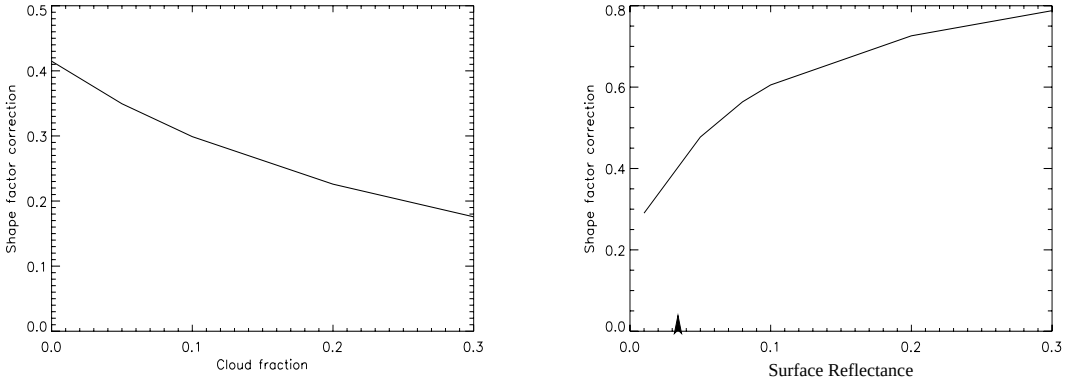

Fig. 10. Shape factor correction sensitivity to cloud irradiance fraction (left panel) and surface reflectance (right panel). Arrows indicate values corresponding to the reference case from the DABEX simulation.

AMTD
6, 6645–6684, 2013

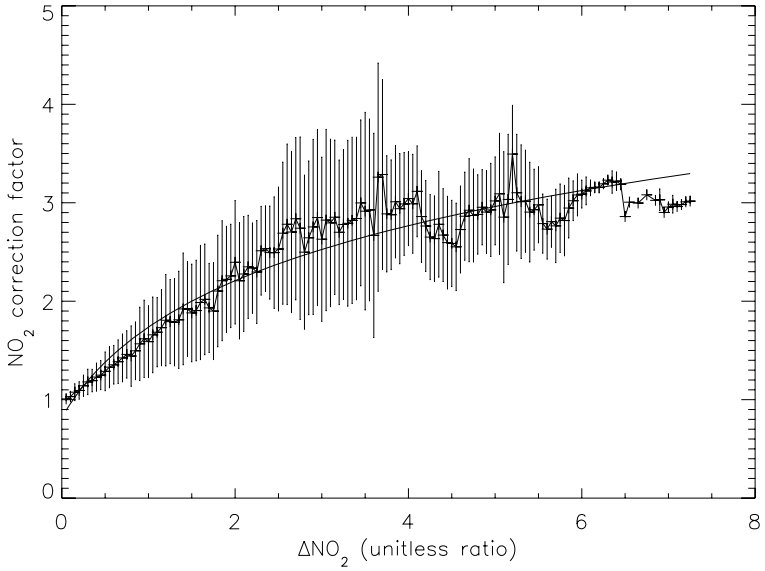

Fig. 11. Relationship between the NO_2 correction factor and ΔNO_2. Vertical bars represent the standard deviation of the NO_2 correction factor within each ΔNO_2 bin. The solid black line represents the logarithmic fit to the curve.

AMTD
6, 6645–6684, 2013

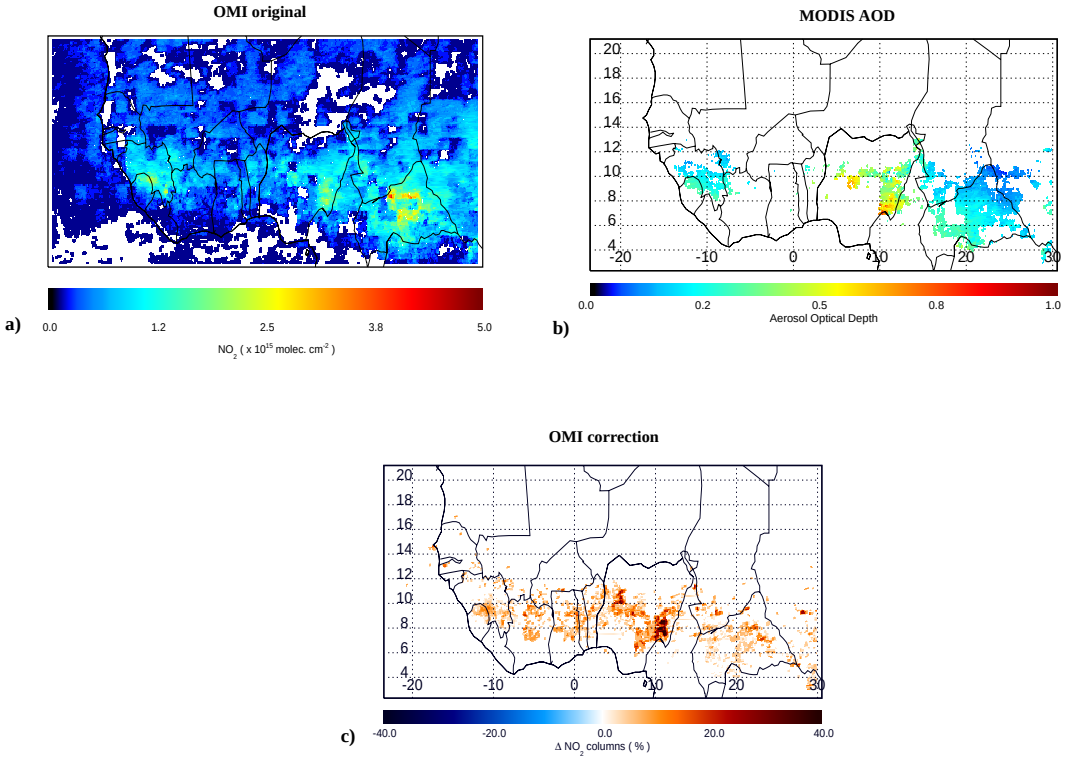

Fig. 12. Mean OMI DP GC tropospheric NO_2 column (original product) **(a)**, mean MODIS aerosol optical depth **(b)**, and mean OMI NO_2 correction factor (%) **(c)** during DABEX. MODIS AODs and NO_2 correction factors are shown only over areas with OMI DP GC NO_2 columns $> 10^{15}$ molec cm^{-2}.

AMTD
6, 6645–6684, 2013